Research Article

Received: 20 April 2015 Revised: 19 June 2015 Accepted article published: 6 July 2015 Published online in Wiley Online Library: 31 July 2015

(wileyonlinelibrary.com) DOI 10.1002/jctb.4769

Modeling and control strategies for anoxic biotrickling filtration in biogas purification

Fernando Almenglo,[a*] Martín Ramírez,[a] José Manuel Gómez,[a] Domingo Cantero,[a] Xavier Gamisans[b] and Antonio David Dorado[b]

Abstract

BACKGROUND: Anoxic biotrickling filters have been used to 'sweeten' biogas. Nevertheless, the cost and availability of large amounts of nitrate could limit the use of this technology in comparison with aerobic biotrickling filters. The development of a dynamic mathematical model would be useful for the design of control strategies with regard to nitrate dosage.

RESULTS: A dynamic model has been developed to describe the performance of an anoxic biotrickling filter for biogas desulfurization. The model considers the most relevant phenomena involved in biotrickling filter operation: advection, absorption, diffusion and biodegradation. Moreover, a fraction of the liquid phase is stagnant – an assumption that increases the importance of diffusion phenomena for low liquid flow rates. Once the model had been validated, six control strategies were analyzed for different scenarios and purposes: i.e. to minimize nitrate consumption and/or to maximize H_2S removal efficiency.

CONCLUSION: The mathematical model developed from the description of the phenomena involved in the process is a powerful tool to evaluate all possible strategies when considering and quantifying the savings and improvements in different operating modes.

Supporting information may be found in the online version of this article.

Keywords: biofiltration of waste gases; biogas; process control; denitrification; modeling

INTRODUCTION

The use of biogas as a renewable energy source is a promising alternative to conventional fossil fuels. However, biogas contains some impurities such as reduced sulfur compounds (RSC), ammonia, siloxanes, aromatics, halogenated compounds and other volatile organic compounds (VOCs).[1] Among these impurities, hydrogen sulfide (H_2S) is the most important RSC and it is present in concentrations between 0.05 and 2% v/v.[2] In recent years, biotrickling filters (BTFs) have been used to 'sweeten' biogas under both aerobic[3–7] and anoxic[6,8–10] conditions.

In anoxic BTFs, nitrate (NO_3^-) or nitrite (NO_2^-) are used as electron acceptors instead of oxygen (O_2). Hence, the advantages of anoxic BTFs over aerobic systems include reduction of the explosion risk, dilution and the negligible mass transfer limitations of nitrate as an electron acceptor.[6,8,11] However, the cost and availability of large amounts of nitrate lead to a slight increase in the treatment cost in comparison with aerobic BTFs.[8] Thus, optimization of nitrate dosing without affecting the abatement efficiency is an important aspect to improve the economic viability of this technique.

The main concern with anoxic BTFs is related to the control strategy with regard to nitrate (or nitrite) dosage. Consequently, it is necessary to optimize the anoxic BTF performance and the development of a rigorous model would be useful for the design of control system strategies. However, to date only empirical models for anoxic BTFs have been developed.[12,13] The application of these models is limited to the specific equipment and conditions for which they were developed. As an alternative, dynamic models were developed to represent the transient phenomena commonly found in the industrial field (start-up and inlet concentration peaks).[14] In these models, the changes in pollutant concentration over time and space are described by a set of partial differential equations for each component.[15]

The development of a dynamic mathematical model provides a better understanding of the fundamental mechanisms that occur in biofiltration and allows the parameters that are most influential in its performance to be identified. Moreover, several operating conditions can be simulated and the experimental time can therefore be minimized, thus avoiding costly modifications to the system.[16] The use of dynamic models for the control of nitrate dosing or for other control strategies has not been studied to date

* *Correspondence to: Fernando Almenglo, Department of Chemical Engineering and Food Technologies, Faculty of Sciences, University of Cadiz, 11510 Puerto Real (Cádiz), Spain. E-mail: fernando.almenglo@uca.es*

a *Department of Chemical Engineering and Food Technologies, Faculty of Sciences, University of Cadiz, 11510, Puerto Real, Cádiz, Spain*

b *Department of Mining Engineering and Natural Resources, Universitat Politècnica de Catalunya, Bases de Manresa 61-73, 08240, Manresa, Spain*

with the aim of improving anoxic BTF operation. The main aim of the work described here was to develop, calibrate and validate a dynamic model for an anoxic BTF by monitoring an industrial plant located at the WWTP 'Bahía Gaditana' (San Fernando, Spain) for year-round operation. The model was developed by the application of mass balances and the definition of the main processes that occur in a BTF: advection, absorption, diffusion and biodegradation.

MATERIAL AND METHODS

Experimental set-up

An anoxic BTF at pilot scale[17] was built and operated for 360 days. The BTF was built from fiberglass-reinforced polyester and the diameter and bed heights were 0.5 and 0.85 m, respectively. The liquid recirculating volume was 0.09 m^3, the treated biogas flow rate ranged between 1 and 5 $m^3\ h^{-1}$ (corresponding to loading rates from 33 to 193 gS $m^{-3}\ h^{-1}$) and the recirculating flow rate was in the range 1–3 $m^3\ h^{-1}$.

Industrial water from the WWTP was used to feed the BTF. This water was supplemented with a nitrate concentrate solution. The composition of the nitrate concentrate solution was: $NaNO_3$ (500 g L^{-1}), KH_2PO_4 (10 g L^{-1}), NH_4Cl (5 g L^{-1}), $MgSO_4{\cdot}7H_2O$ (4 g L^{-1}), trace element solution SL–4 (5 mL L^{-1}) and a solution of $FeSO_4{\cdot}7H_2O$ (2 g in 1 L of H_2SO_4 0.1 N) (10 mL L^{-1}). The composition of trace element solution SL–4 was: EDTA (0.5 g L^{-1}), $FeSO_4{\cdot}7H_2O$ (0.2 g L^{-1}) and trace element solution SL–6 (100.0 mL L^{-1}). This trace element solution SL – 6 was composed of (g L^{-1}): $ZnSO_4{\cdot}7H_2O$ (0.1), $MnCl_2{\cdot}4H_2O$ (0.03), H_3BO_3 (0.3), $CoCl_2{\cdot}6H_2O$ (0.2), $CuCl_2{\cdot}2H_2O$ (0.01), $NiCl_2{\cdot}6H_2O$ (0.02), $Na_2MoO_4{\cdot}H_2O$ (0.03).

A digital Multimeter 44 (Crison Instruments, Spain) was used for oxidation–reduction potential (ORP) measurement and pH control at 7.4, which was achieved by the addition of NaOH (48/50% (weight/weight), Haupold, Spain). The H_2S concentration in the biogas stream was measured using a gas chromatograph with a thermal conductivity detector (GC-450, Bruker, Germany). A specific gas sensor (GasBadge® Pro, Industrial Scientific, USA) was used for H_2S concentrations below 500 ppm_V. Sulfate, nitrite, nitrate, total solids and total organic nitrogen were determined according Clesceri *et al.*[18]

BTF operational period

Several studies were performed in the anoxic BTF operational period. First, the start-up stage and three regimes for nitrate supply were evaluated, namely manual, continuous and controlled by ORP.[17] Second, the effect of biogas flow rate and recirculation medium were tested.[12] Third, a comparison was made between two flow operation modes, namely co-current and counter-current.[19]

The model was calibrated by studying the effect of changes in the flow rate of biogas and recirculation medium[12] in the period from day 173 to 224, the mean inlet H_2S concentration was 6.08 ± 0.46 gS Nm^{-3}. For the validation stage, in order to corroborate that the model was able to describe general operation of anoxic BTFs, three independent and separate operational periods, without failures, were selected. The first period was from day 135 to day 146 (mean inlet H_2S concentration equal to 6.61 ± 0.36 gS Nm^{-3}),[17] the second period was from day 230 to day 242 (mean inlet H_2S concentration equal to 5.74 ± 0.53 gS Nm^{-3})[19] and the third period was on day 293 (inlet H_2S concentration equal to 5.81gS Nm^{-3}).[19] The nitrate solution (500 g $NaNO_3$ L^{-1}, BASF, Germany) was added in discontinuous mode and this process was automated by ORP. The ORP is directly related to the ion concentrations in an aqueous medium. It was observed experimentally that the ORP value remained almost constant when nitrate is present in the recirculating liquid. Conversely, when the nitrate was depleted the ORP drastically decreased. The latter behavior is attributed to sulfide accumulation due to electron acceptor exhaustion. When the anoxic BTF system is working properly, the increase in sulfide concentration (or decrease in ORP) is caused by the depletion of nitrate (Fig. S1). Therefore, when the ORP reaches the set-point (−360 mV) two sequential steps begin. First, the discharge valve is open for the time necessary to purge the desired volume. Second, when the purge is finished, the pump for the nitrate solution and the industrial water feed valve are simultaneously activated. The pump for the nitrate worked for a fixed time in order to achieve the desired nitrate concentration in the recirculation liquid. The feed valve was open until the working volume was reached. After the nitrate supply had finished, the ORP returned to normal (set-point) values.

Simultaneous autotrophic desulfurization and denitrification can occur through complete or partial reaction and this results in the formation of sulfate and nitrogen gas (for complete reaction) or elemental sulfur and nitrite (for partial reaction).[20] The production of elemental sulfur, by partial desulfurization, depends on the ratio of supplied nitrate and sulfide removed and this has a linear relationship.[8] The production of nitrite in the pilot anoxic BTF was below the inhibition concentration (33.3 $gN-NO_2^-\ m^{-3}$).[21] The nitrite concentration was between 0.1 and 10 $gN-NO_2^-\ m^{-3}$ in the calibration stage, between 0.2 and 16.0 $gN-NO_2^-\ m^{-3}$ in the first validation stage and between 0.3 and 21.3 $gN-NO_2^-\ m^{-3}$ in the 2nd and 3rd validation stages. Furthermore, Mora *et al.*[21] found that the anoxic sulfide-oxidizing culture had a high denitrification activity. Hence, partial and complete desulfurization and complete denitrification were considered. The partial equations for the complete denitrification with sulfide as electron donor were described by Mora *et al.*[21] (Equations (1) and (2)). This study was performed in a continuous stirred tank reactor (CSTR) of 4.2 L (pH 7.5 and 30 °C), and sulfide and nitrate loading rates of 8.6 gS m^{-3} reactor h^{-1} and a 4.5 gN m^{-3} reactor h^{-1}, respectively. In their study, the authors found that the microbial diversity was preserved during the CSTR operation.

$$HS^- + 0.35NO_3^- + 0.013NH_4^+ + 0.059HCO_3^- + 1.40H^+ + \\ +0.004CO_2 \rightarrow 0.013C_5H_7O_2N + 0.175N_2 + S^0 + 1.21H_2O \quad (1)$$

$$S^0 + 0.876NO_3^- + 0.080NH_4^+ + 0.379HCO_3^- + 0.023CO_2 + \\ +0.343H_2O \rightarrow 0.080C_5H_7O_2N + 0.44N_2 + SO_4^{2-} + 0.824H^+ \quad (2)$$

Model assumptions

The main assumptions made for the model were based on those commonly made in previous biotrickling filter models,[15,22–25] and adapted to the anoxic BTF. The model presented herein includes the following assumptions:

1 The biofilm is completely developed over the carrier, is homogeneously distributed along the bed height and is fully wetted.
2 The liquid phase is considered to be divided into two fractions: flowing and stagnant (both of which can be considered as

liquid hold-up). Moreover, both fractions are homogeneously distributed along the bed height.

3 The area fraction in contact with the flowing liquid phase (α) is related to the liquid flow rate by a linear function.
4 The liquid layer thickness is constant, for both liquid phases and along the bed, for each F_L.
5 Mass transfer between flowing liquid and stagnant liquid, and between liquid phases and biofilm are described by diffusion phenomena.
6 The H_2S mass transfer in the gas–liquid interface occurs in both liquid phases, i.e. flowing and stagnant, and is defined by Ondas's equation.[26]
7 The adsorption of the chemical species on the support surface is negligible.
8 The axial flows (gas and flowing liquid) are described by a plug-flow model.
9 Mass transport into the biofilm is described by diffusion (Fick's law).
10 The biomass-substrate yields in the biofilm are equal to those described by Mora *et al.*[21] for suspended cultures.
11 Sulfide and elemental sulfur oxidizing kinetics in the biofilm are equals to those described by Mora *et al.*[21] for suspended cultures.
12 The biological reaction only occurs in the biofilm; there is a negligible amount of suspended biomass in the liquid recirculating volume.
13 The effect of pH is only considered to calculate the H_2S dissociation in the liquid phase. The effect of pH on the biological activity is neglected because all experiments were conducted at constant pH (same value used by Mora *et al.*[21] for kinetics determination).

The model describes the dynamic of the main species involved in an anoxic BTF (H_2S concentration in the gas, liquid and biofilm phases; nitrite and sulfate concentrations in the liquid and biofilm phases and the elemental sulfur production in the biofilm). The system of partial differential equations was solved by discretizing the height and biofilm thickness, thus converting them to ordinary differential equations. The scheme for the model and the discretization along the bed and within the biofilm is shown in Fig. 1,

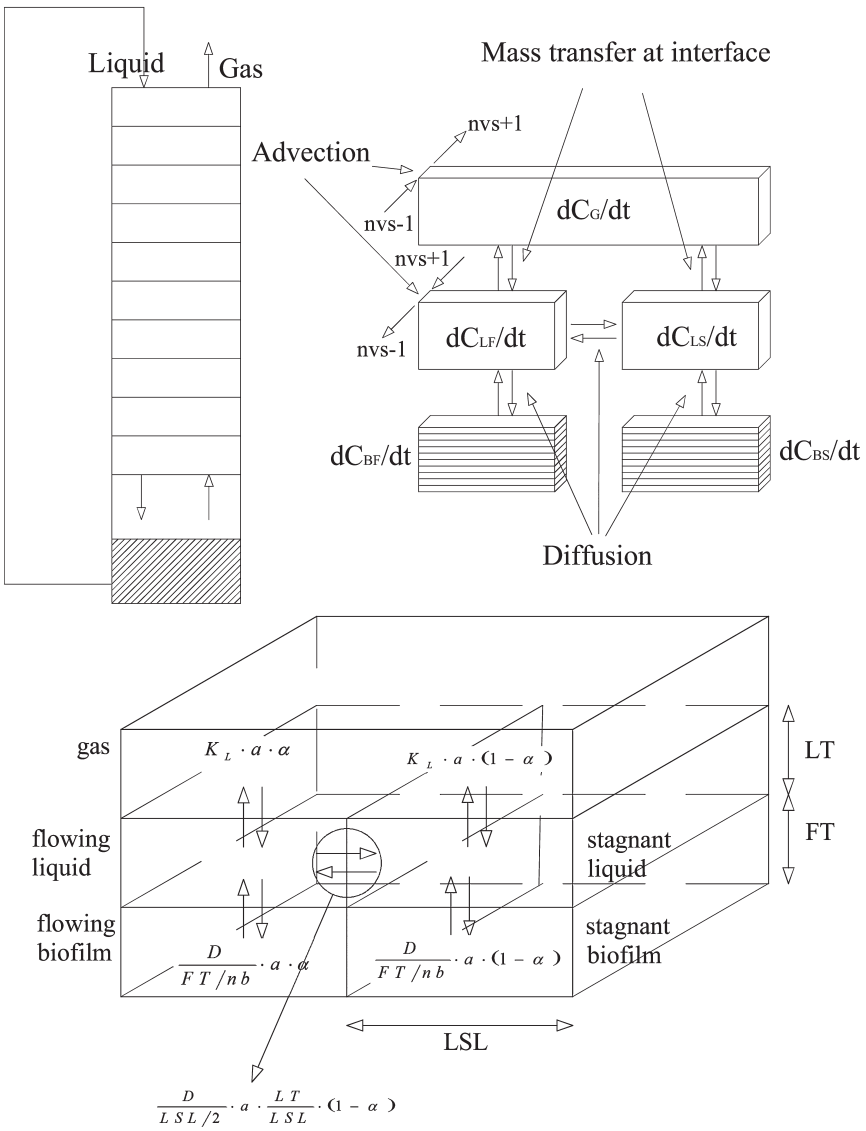

Figure 1. Model scheme and discretization.

Table 1. Model symbols

Parameters	Description	Parameters	Description
a	specific bed surface ($m^2\ m^{-3}$)	k_G	gas individual mass transfer coefficient ($m\ h^{-1}$)
a_p	specific packing surface ($m^2\ m^{-3}$)	k_{SL}	stagnant liquid individual mass transfer coefficient ($m\ h^{-1}$)
C	concentration ($g\ m^{-3}$)	LSL	length of the stagnant liquid layer (m)
C^*	equilibrium concentration ($g\ m^{-3}$)	LT	liquid thickness (m)
D	diffusivity ($m^2\ h^{-1}$)	M	total number of experiments used
Er	packing efficiency number (–)	m	dimensionless gas–liquid equilibrium constant (–)
F	volumetric flow rate ($m^3\ h^{-1}$)	N	total number of data sets for each experiment
FT	biofilm thickness (m)	nb	number of biofilm layers
g	gravitational constant ($m\ s^{-2}$)	nvs	number of bed height layers
H	Henry's law constant (–)	R	reaction rate ($g\ m^{-3}\ h^{-1}$)
K	inhibition constant for sulfur oxidation ($g\ m^{-3}$)	Re	Reynolds number (–)
$K_{iS,H2S}$	constant for sulfide inhibition ($g\ m^{-3}$)	Sc	Schmidt number (–)
K_G	gas overall mass transfer coefficient ($m\ h^{-1}$)	Sh	Sherwood number (–)
K_L	liquid overall mass transfer coefficient ($m\ h^{-1}$)	t	time (h)
$K_{S,H2S}$	affinity constant for sulfide ($g\ m^{-3}$)	V	volume (m^3)
$K_{S,NO3}$	affinity constant for nitrate ($g\ m^{-3}$)	V_{1c}	volume of one packing cube (m^3)
$K_{S,S0}$	affinity constant for sulfur ($g\ m^{-3}$)	$V_{b,1c}$	biofilm volume in one packing cube (m^3)
k_{a1}	first H_2S dissociation constant (–)	X	biomass concentration ($gN\ m^{-3}$)
k_{a2}	second H_2S dissociation constant (–)	Y	yield (–)
k_{FL}	flowing liquid individual mass transfer coefficient ($m\ h^{-1}$)	z	linear dimension of the column
Greek letters			
α	flowing liquid fraction (–)	μ	viscosity (Pa s)
p_α	proportionality constant	ρ	density ($kg\ m^{-3}$)
ε	gas volume fraction (–)	φ	liquid volume fraction (–)
Subscripts			
b	biofilm	$NO3$	nitrate
D	purge	OUT	outlet
Fb	'flowing' biofilm	P	packing material
FL	flowing liquid	RL	recirculating liquid
G	gas	$S0$	elemental sulfur
$H2S$	hydrogen sulfide	Sb	'stagnant' biofilm
IN	inlet	SL	stagnant liquid
k	index for chemical species	$SO4$	sulfate
L	liquid	T	total
MM	nitrate concentrated solution	W	water
Superscripts			
EXP	experimental		

each subdivision is ideally mixed. The bed height and biofilm thickness were divided into 'nvs' and 'nb' slices, respectively, and the discretization was optimized to reduce the computational resolution time. The numerical solution was obtained using MATLAB 7.7 (Mathworks, Natik, MA). The main equations for the model are listed in the following section.

Mass balances

The main mass balances are described by the following equations. Table 1 provides a description of the model symbols. The conceptual scheme is represented in Fig. 1, in which the relationship between phases (gas, liquids and biofilms) is shown along with the transport phenomena between phases and the coefficients used in the interfacial mass transfer.

The model equation for the bulk gas phase describes advective transport and mass transfer between gas and liquid phases. The gas–liquid mass transfer occurs in both liquid phases, considering the specific area in contact with the flowing liquid phase ($a{\cdot}\alpha$) and with the stagnant liquid phase ($a{\cdot}(1-\alpha)$).

$$\left.\frac{dC_{G,H_2S}}{dt}\right| = -v_G\frac{\partial C_{G,H_2S}}{\partial z} - \frac{a}{\varepsilon}\cdot K_{FL,H_2S}\cdot\alpha\cdot\left(C^*_{FL,H_2S} - C_{FL,H_2S}\right) - \\ -\frac{a}{\varepsilon}\cdot K_{SL,H_2S}\cdot(1-\alpha)\cdot\left(C^*_{SL,H_2S} - C_{SL,H_2S}\right) \quad (3)$$

with the following boundary conditions:

$$\text{for } z = 0, C_G = C_{G,IN};$$

$$\text{for } t = 0, C_G = 0.$$

The flowing liquid phase is in contact with the gas phase, the stagnant liquid phase and the biofilm. These phenomena can be

described as follows:

$$\frac{dC_{FL,k}}{dt} = v_z\frac{\partial C_{FL,k}}{\partial z} + \frac{a}{\varphi_F}K_{FL,k}\cdot\alpha\cdot\left(C^*_{FL,k} - C_{FL,k}\right) - \\ -\frac{a}{\varphi_F}\cdot(1-\alpha)\cdot\frac{D_{L,k}}{(LSL/2)}\cdot\frac{LT}{LSL}\cdot\left(C_{FL,k} - C_{SL,k}\right) \\ -\frac{a}{\varphi_F}\frac{D_{L,k}}{(FT/nb)}\cdot\alpha\cdot\left(C_{FL,k} - C_{Fb,k,1}\right) \quad (4)$$

The second term in Equation (4), which describes mass transfer at the gas–liquid interface, is valid only for H_2S because the model does not consider gas–liquid transfer for nitrate, sulfate and elemental sulfur. The third term describes the diffusion at the 'flowing' and 'stagnant' liquid interfaces using Fick's law; this term considers the specific interfacial area as $(a\cdot(1-\alpha)\cdot LT/LSL)$ and the average length as $(LSL/2)$; in which LT is the liquid thickness and LSL is the stagnant liquid length (Fig. 1). The mass transfer between the flowing liquid and the biofilm is described in the fourth term, in which the specific flowing area is used $(a\cdot\alpha)$ and the length (FT/nb) considers the biofilm division. The boundary conditions were:

$$\text{for } z = z_{max}, C_L = C_{L,REC};$$
$$\text{for } t = 0, C_{FL} = 0.$$

The stagnant liquid phase is described by similar phenomena, excluding advective transport.

$$\frac{dC_{SL,k}}{dt} = \frac{a}{\varphi_S}K_{SL,k}\cdot(1-\alpha)\cdot\left(C^*_{SL,k} - C_{SL,k}\right) + \\ +\frac{a}{\varphi_S}\cdot(1-\alpha)\cdot\frac{D_{L,k}}{(LSL/2)}\cdot\frac{LT}{LSL}\cdot\left(C_{FL,k} - C_{SL,k}\right) \\ -\frac{a}{\varphi_S}\frac{D_{L,k}}{(FT/nb)}\cdot(1-\alpha)\cdot\left(C_{SL,k} - C_{Sb,k,1}\right) \quad (5)$$

with the boundary condition:

$$\text{for } t = 0, C_{SL} = 0.$$

Mass balances in the biofilm are divided into 'flowing biofilm' (which is in contact with flowing liquid, Equation (6)) and 'stagnant biofilm' (which is in contact with stagnant liquid, Equation (7)). The mass transfer is due to diffusional processes and is described by Fick's law. Moreover, the biological reactions (Equations (17) and (18)) occur in both biofilms.

$$\frac{dC_{Fb,k}}{dt} = D_{b,k}\frac{\partial^2 C_{Fb,k}}{\partial x^2} - Y_{k/H_2S}R_{H_2S,Fb} - Y_{k/S^0}R_{S^0,Fb} \quad (6)$$

$$\frac{dC_{Sb,k}}{dt} = D_{b,k}\frac{\partial^2 C_{Sb,k}}{\partial x^2} - Y_{k/H_2S}R_{H_2S,Sb} - Y_{k/S^0}R_{S^0,Sb} \quad (7)$$

The mass balance in the recirculating volume is described by Equation (8) for the concentration in the recirculated liquid and by Equation (9) for the volume of the recirculated liquid.

$$\frac{dC_{RL,k}}{dt} = \frac{F_L}{V_R}\left(C_{FL,k,1} - C_{RL,k}\right) + \frac{F_{MM}}{V_R}C_{MM,k} - \frac{F_P}{V_R}C_{RL,k} + \frac{F_W}{V_R}C_{W,k} \quad (8)$$

$$\frac{dV_R}{dt} = F_{MM} - F_P + F_W \quad (9)$$

Determination of mass transfer coefficients

Onda's equations[26] were used to calculate the local individual liquid (k_L) and gas (k_G) mass transfer coefficients. In Equation (10), the area in contact with the flowing liquid ($a\cdot\alpha$) was used instead of the wetted area described by Onda *et al.*:[26]

$$k_G = 5.23\cdot a\cdot D_G\cdot \mathrm{Re}_G^{0.7}\cdot Sc_G^{1/3}\cdot Er^2 \quad (10)$$

$$k_{FL} = 0.0051\cdot\left(\frac{L_F}{(a\cdot\alpha)\cdot\mu_L}\right)^{2/3}\cdot Sc_L^{-1/2}\cdot Er^{-0.4}Sh_L^{-1/3} \quad (11)$$

The individual mass transfer coefficient for the stagnant liquid was calculated using an equation similar to Equation (11). In this equation, the stagnant area $(a\cdot(1-\alpha))$ was considered instead of the flowing area (Equation (12)).

$$k_{SL} = 0.0051\cdot\left(\frac{L_F}{(a\cdot(1-\alpha))\cdot\mu_L}\right)^{2/3}\cdot Sc_L^{-1/2}\cdot Er^{-0.4}Sh_L^{-1/3} \quad (12)$$

Overall mass transfer coefficients were obtained with the following well-known expression, using the dimensionless gas–liquid equilibrium constant (m):

$$\frac{1}{mK_Ga} = \frac{1}{K_{FL}(a\cdot\alpha)} = \frac{1}{k_{FL}(a\cdot\alpha)} + \frac{1}{mk_G(a\cdot\alpha)} \quad (13)$$

$$\frac{1}{mK_Ga} = \frac{1}{K_{SL}(a\cdot(1-\alpha))} = \frac{1}{k_{SL}(a\cdot(1-\alpha))} + \frac{1}{mk_G(a\cdot(1-\alpha))} \quad (14)$$

It is necessary to consider the dissociation of H_2S in the liquid phase and the concentrations of the dissociated species depend on the pH (Equations (15) and (16)).

$$H_2S_{(g)} \leftrightarrow H_2S_{(aq)} \overset{ka1}{\longleftrightarrow} HS^-_{(aq)} + H^+ \overset{ka2}{\longleftrightarrow} S^{2-}_{(aq)} + 2H^+ \quad (15)$$

$$m = \frac{C_{H_2S,g}}{C_{H_2S,aq} + C_{HS^-,aq} + C_{S^{2-},aq}} = \frac{H}{1 + \frac{k_{a1}}{10^{-pH}} + \frac{k_{a1}\cdot k_{a2}}{10^{-2\cdot pH}}} \quad (16)$$

Biological reaction rates

The kinetic model proposed by Mora *et al.*[21] was used and this concerned a sulfide oxidant/nitrate reducing mixed culture obtained from the anoxic BTF.[19] For sulfide oxidation a multi-substrate equation was employed and this included a Haldane-type term to describe substrate inhibition by sulfide, while a Monod-type term was used to describe the nitrate contribution (Equation (17)). For the elemental sulfur oxidation two Monod-type terms were used for both elemental sulfur and nitrate, along with an inhibition term that considered sulfide (Equation (18)).

The biomass concentration (X) (gN m^{-3}) was considered to be constant along the bed. The biomass-substrate yields ($Y_{X/H2S}$ and $Y_{X/S0}$) (gN $(gS)^{-1}$) were estimated according to Equations (1) and (2).

$$R_{H_2S,b,i,j} = \mu_{MAX,H_2S}\cdot\left(\frac{1}{Y_{X/H_2S}}\right)\cdot\left(\frac{C_{bH_2S,i,j}}{K_{S,H_2S} + C_{bH_2S,i,j} + \frac{\left(C_{bH_2S,i,j}\right)^2}{K_{iS,H_2S}}}\right)\cdot \\ \cdot\left(\frac{C_{bNO_3,i,j}}{K_{S,NO_3} + C_{bNO_3,i,j}}\right)\cdot X \quad (17)$$

Table 2. Parameters used in the calibration stage

Parameter	Value	Description
a	359.5	specific bed surface ($m^2\ m^{-3}$)
a_P	600	specific packing surface ($m^2\ m^{-3}$)
$D_{G,H2S}$	$1.80 \cdot 10^{-4}$	H_2S diffusivity in biogas[27,28] ($m^2\ h^{-1}$)
$D_{L,H2S}$	$8.58 \cdot 10^{-6}$	H_2S diffusivity in water[29] ($m^2\ h^{-1}$)
$D_{L,NO3}$	$7.61 \cdot 10^{-6}$	NO_3^- diffusivity in water[29] ($m^2\ h^{-1}$)
$D_{L,SO4}$	$4.26 \cdot 10^{-6}$	SO_4^{2-} diffusivity in water[30] ($m^2\ h^{-1}$)
F_W	5	volumetric flow for water ($m^3\ h^{-1}$)
F_{MM}	$7.9 \cdot 10^{-3}$	volumetric flow for nitrate solution ($m^3\ h^{-1}$)
FT	$4.17 \cdot 10^{-4}$	biofilm thickness (m)
g	9.81	gravitational constant ($m\ s^{-2}$)
gN_P	0.068	grams of nitrogen in biomass by packing gram ($gN\ g^{-1}$)
gP	2289.36	packing grams in bed (g)
H	0.518	Henry's law constant (30 °C) [31] (–)
K	5.13	inhibition constant for sulfur oxidation[21] ($gS\ m^{-3}$)
$K_{iS,H2S}$	78.1	constant for sulfide inhibition[21] ($gS\ m^{-3}$)
$K_{S,H2S}$	8.4	affinity constant for sulfide[21] ($gS\ m^{-3}$)
$K_{S,NO3}$	1.3	affinity constant for nitrate[21] ($gN\text{-}NO_3\ m^{-3}$)
$K_{S,S0}$	0.609	affinity constant for sulfur[21] ($gS\ m^{-3}$)
k_{a1}	$9.1\ 10^{-8}$	first H_2S dissociation constant[32] (–)
k_{a2}	$1.1\ 10^{-12}$	second H_2S dissociation constant[32] (–)
m	0.1579	gas–liquid equilibrium constant
$Y_{NO3/H2S}$	0.1531	yield of NO_3 and H_2S (equation 1) ($gN\text{-}NO_3\ (gS)^{-1}$)
$Y_{NO3/S0}$	0.3832	yield of NO_3 and S^0 (equation 2) ($gN\text{-}NO_3\ (gS)^{-1}$)
$Y_{X/H2S}$	0.00568	yield of biomass and H_2S (equation 1) ($gN\ (gS)^{-1}$)
$Y_{X/S0}$	0.035	yield of biomass and S^0 (equation 2) ($gN\ (gS)^{-1}$)
μ_G	$1.89\ 10^{-5}$	biogas viscosity[33] (Pa s)
μ_L	$8.20\ 10^{-4}$	water viscosity (Pa s)
$\mu_{MAX,H2S}$	0.126	maximum growth rate for equation 17[21] (h^{-1})
$\mu_{MAX,S0}$	0.199	maximum growth rate for equation 17[21] (h^{-1})
ρ_G	1.094	biogas density[33] ($kg\ m^{-3}$)
ρ_L	995.7	water density ($kg\ m^{-3}$)

$$R_{S^0,b,i,j} = \mu_{MAX,S^0} \cdot \left(\frac{1}{Y_{X/S^0}}\right) \cdot \left(\frac{C_{bS^0,i,j}}{K_{S,S^0} + C_{bS^0,i,j}}\right) \cdot \left(\frac{C_{bNO_3,i,j}}{K_{S,NO_3} + C_{bNO_3,i,j}}\right) \cdot \left(\frac{K}{K + C_{bH_2S,i,j}}\right) \cdot X \quad (18)$$

Model calibration

The parameters that describe the anoxic BTF are given in Table 2. The specific bed surface was calculated according to Equation (19) – this equation relates the specific packing surface, the packing volume and total volume of the bed. The biofilm thickness was estimated from the measured biomass volume (31.27 cm^3), contained in a packing cube (125 cm^3), and the specific packing surface (600 $m^2\ m^{-3}$) (Equation (20)). The total organic nitrogen, in a cube of packing, was 0.068 gN (g packing)$^{-1}$. The biomass concentration was estimated by considering a planar geometry for the biomass volume (Equations (21) and (22)). The liquid volume and the purge flow rate were experimentally estimated as a function of the liquid flow rate (Equations (23) and (24)). The liquid layer thickness was calculated as a function of the liquid volume, supposing planar geometry (Equation (25)). The flowing liquid fraction (α) was considered as a linear function of the liquid flow rate (Equation (26)).

$$a = a_P \frac{V_P}{V_T} \quad (19)$$

$$FT = \frac{V_{b,1c}}{V_{1c} \cdot a_P} \quad (20)$$

$$gN_b = gN_P \cdot gP \quad (21)$$

$$X = \frac{gN_b}{a \cdot V_T \cdot FT} \quad (22)$$

$$V_L = \left(4.27 - 2.14 \cdot F_L\right) \cdot 10^{-3} \quad (23)$$

$$F_D = 2.41 - 0.46 \cdot F_L \quad (24)$$

$$LT = \frac{V_L}{a \cdot V_T} \quad (25)$$

$$\alpha = p_\alpha \cdot F_L \quad (26)$$

The developed model was calibrated by means of only two parameters and these are difficult to determine experimentally: the length of the stagnant liquid layer (LSL) and the proportional coefficient (p_α) for the flowing fraction calculation. The deviations in the H_2S outlet concentration between experimental data and those predicted by the model were used to obtain these parameters. Therefore, the objective function (OF) to minimize for each period simulated was:

$$OF = \sum_{j=1}^{M} \sqrt{\sum_{i=1}^{N} \left[C_{G,OUT}\left(LSL, p_\alpha\right) - C_{G,OUT}^{EXP}\right]^2} \quad (27)$$

Control strategies

Six control strategies (CS) for dosing the nitrate solution were proposed (Table 3) and the control variables were the concentration of H_2S in the gas outlet and/or sulfide in the recirculated liquid. Two dosing modes for the nitrate solution were evaluated, namely discontinuous mode and continuous mode. In discontinuous mode two sequential steps occur: (i) the purge of the recirculated liquid; and (ii) the dosage of the nitrate and industrial water up to

Table 3. Summary of the control strategies

CS	Nitrate solution dosage	Biogas flowrate	Set point [$gS\ m^{-3}$]
CS#A	Discontinuous	Constant	$C_{LREC,H2S} < 10$
CS#B	Discontinuous	Constant	$C_{OUT,H2S} < 0.4$
CS#C	Continuous	Constant	$C_{OUT,H2S} \leq 0.4$
CS#D	Continuous	Constant	$C_{LREC,H2S} \leq 5$
CS#E	Discontinuous	Variable	$C_{LREC,H2S} < 10$
CS#F	Discontinuous	Variable	$C_{OUT,H2S} < 0.4$ g

the working volume. In continuous mode the nitrate solution was added continuously and its flow rate was varied to maintain the set-point of the controlled variable. Similarly, the industrial water flow was constant in order to keep the sulfate concentration below the desired value. For all the CSs the recirculation flow rate was 3 $m^3\ h^{-1}$, the simulated period was 100 h (i.e. longer than a complete cycle) and the volume purged was ten times the volume of the nitrate concentrate solution. It was considered that the inlet H_2S concentrations fluctuated with time in order to represent the behavior of an industrial effluent by means of a sine function. The conditions for all CSs were within the calibration range: the calibration liquid flow rate was between 1 and 3 $m^3\ h^{-1}$, the input load was between 20.1 and 176.5 gS $Nm^{-3}\ h^{-1}$ and the nitrate concentration between 1.4 and 423.7 gN – NO_3^- m^{-3}. Likewise, the liquid flow rate and the input load were within the range of the validation experiments; liquid flow rate of 1.5 and 3 $m^3\ h^{-1}$ and input load between 35 and 193 gS $Nm^{-3}\ h^{-1}$. To evaluate the most appropriate CS, the average and maximum H_2S concentrations in the outlet gas, the total nitrate consumption and the total nitrate purged were considered as target variables.

In CS#A the nitrate dosage was discontinuous and the sulfide concentration in the recirculating liquid was used as a control variable. In CS#B the dosage was also discontinuous but the outlet H_2S concentration in the biogas was used as a control variable. As the set-point a value of 0.4 gS Nm^{-3} (around 300 ppm_V) was selected and this set-point is below the limit required in cogeneration engines (500–800 ppm_V, depending on the manufacturer). In both cases, the maximum nitrate concentration was established as 2000 gN – NO_3^- m^{-3}.

In CS#C and CS#D, the nitrate solution dosage was carried out in continuous mode. In CS#C the flow of the nitrate solution was varied according to the outlet H_2S concentration; the set-point was established to maintain an outlet H_2S concentration of 0.4 gS Nm^{-3}. However, in CS#D the sulfide concentration in the recirculating liquid was the control objective and it was established at 5 gS m^{-3}.

In CS#E and CS#F a variable biogas flow rate was evaluated with discontinuous nitrate dosage used once again, with the same set-points as in CS#A and CS#B, respectively. The variable biogas flow rate was controlled by the outlet H_2S concentration. This control mode keeps the outlet H_2S concentration equal to 0.36 gS Nm^{-3} (90% of H_2S concentration used as the set-point for CS#B, CS#C and CS#F) and the minimum biogas flow rate was 1 $m^3\ h^{-1}$.

RESULTS AND DISCUSSION

Model calibration and validation

The values for the parameters obtained in the calibration step were 2.43×10^{-3} m for *LSL* and 0.19 h m^{-3} for p_α. The model fitting, for the 9 experiments selected, using the estimated parameters is shown in Fig. 2. It can be seen that the outlet H_2S concentration and the nitrate concentration are close to the experimental values. The temperature effect was simulated and it was not

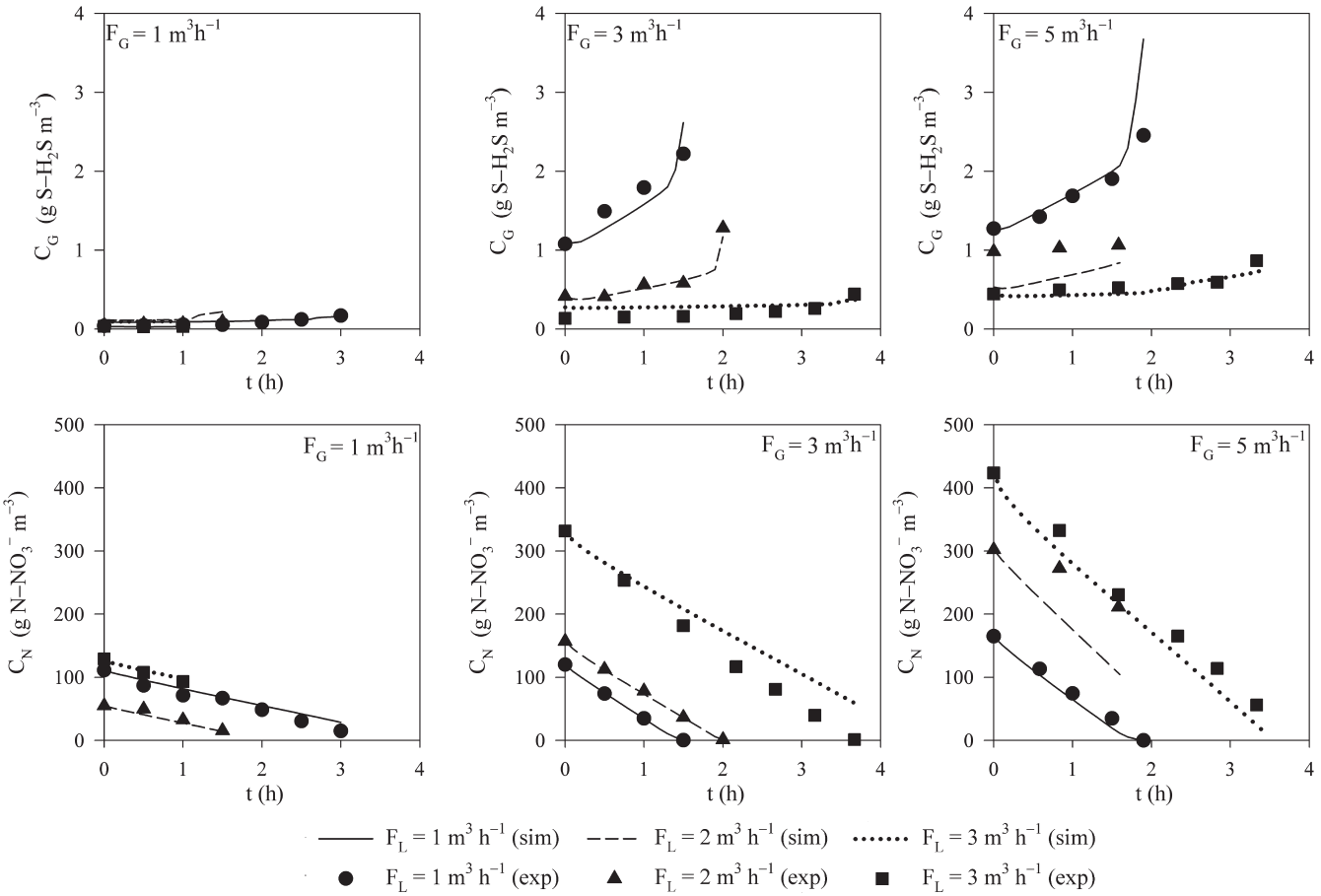

Figure 2. Model calibration. Experimental and simulated data. Upper graphs: outlet H_2S concentration. Lower graphs: nitrate concentration in the recirculation liquid.

significant (Fig. S2). The largest difference between the simulated and experimental data was found at a biogas flow rate of 5 $m^3\ h^{-1}$ and a liquid flow rate of 2 $m^3\ h^{-1}$, where the mean divergence was 0.36 gS Nm^{-3}. The mean difference between experimental and simulated values for a biogas flow rate of 3 $m^3\ h^{-1}$ and a liquid flow rate of 1 $m^3\ h^{-1}$ was 0.20 gS Nm^{-3}. For the other cases the mean difference was less than 0.08 gS Nm^{-3}.

In terms of RE (%), the differences obtained were less than 1% when the biogas flow was 1 $m^3\ h^{-1}$ and they were below 2% for the remaining cases, with the exception of flow rates of 5 $m^3\ h^{-1}$ of biogas and 2 $m^3\ h^{-1}$ of liquid, which gave a value of 6%, and for 3 $m^3\ h^{-1}$ of biogas and 1 $m^3\ h^{-1}$ of liquid, which gave a value of 4%. A Friedman test was performed to evaluate the goodness of fit between experimental and simulated H_2S concentrations, giving values for the *P*-value and R^2 of 1.2×10^{-4} and 0.99, respectively. Regarding to nitrate concentration, the Friedman test parameters were 2.0×10^{-4} and 0.97, respectively.

A sequence to emulate the automatic dosage for the nitrate solution was programmed in MATLAB. There are numerous species that contribute to the ORP value and it is difficult to consider all of these when modeling the ORP. As a result, the concentration of sulfide in the recirculation liquid was used instead of ORP and the set-point was 10 gS m^{-3}.

A comparison between experimental data and the model predictions in the validation step is shown in Fig. 3. The first set of experimental data used in the validation are represented in Fig. 3(A), where the liquid flow rate was 1.5 $m^3\ h^{-1}$ and the biogas flow rate was increased from 1 to 2.8 $m^3\ h^{-1}$; the maximum nitrate concentration was 2100 gN-NO_3^- m^{-3}. In this set of experiments, a period without biogas feeding was also simulated between hour 143 and hour 240. The second set of validation data are shown in Figure 3(B), where the liquid flow rate was 3 $m^3\ h^{-1}$ and the biogas flow rate was increased from 1 to 5.2 $m^3\ h^{-1}$; the maximum nitrate concentration was 350 gN-NO_3^- m^{-3}. The Figure 3(C) shows the third set of experimental data used in the validation, where the liquid flow rate was 3 $m^3\ h^{-1}$, the biogas flow rate was ranged between 1 and 5 $m^3\ h^{-1}$ and the start nitrate concentration was 1400 gN-NO_3^- m^{-3}. Fluctuations in the inlet conditions were observed, mainly because the biogas composition was not controlled. Inlet H_2S concentration and the liquid and biogas flow rates were introduced in the model as input parameters.

The range of simulated nitrate concentrations was between 0.18 and 2127 gN-NO_3^- m^{-3} for the first set of validation data and between 0.03 and 357 gN-NO_3^- m^{-3} for the second set of validation data. Furthermore, the simulated sulfate concentration was between 3749 and 8467 gS-SO_4^{2-} m^{-3} and 4966 and 9072 gS-SO_4^{2-} m^{-3}, for the first and the second validation, respectively. The experimental data were between 3219 and 9062 gS-SO_4^{2-} m^{-3} and 5851 and 8684 gS-SO_4^{2-} m^{-3}. The uncertainty in the initial elemental sulfur in the packing bed (not measured) could explain the divergence between simulated and experimental values. Instead, the third validation set of data (Figure 3(C)) shows an increased goodness of fit of nitrate and sulfate concentration. The mean difference between experimental values and simulated was $4.0\% \pm 2.5\%$ and $1.6\% \pm 1.3\%$ for nitrate and sulfate, respectively. The key parameter to be simulated was the outlet H_2S concentration, because this is the target compound to be removed. If the prediction of the outlet H_2S concentration were imprecise the proposed model would be useless. Better predictions could be achieved with an improved knowledge of the initial elemental sulfur content in the packing material since this parameter has a high sensitivity in model predictions, mainly with respect to the nitrate consumption rate and sulfate production rate.

A Friedman test was carried out to quantify the differences between the experimental data and those predicted by the model. In this case, the *P*-value and R^2 were 0.021 and 0.91, respectively. This result indicates that the difference between the concentrations of H_2S measured experimentally and those simulated by the model were not statistically significant. Figure 4 presents each experimental RE value against the simulated data in order to show a more representative idea of the goodness of fit. Most of the results are included in the 95% confidence level and the average error between simulated and experimental values is 2.8%.

Thus, the model predictions were satisfactory to describe the performance of the anoxic BTF.

In order to obtain an appropriate model it is necessary to simulate correctly the influence of both the nitrate concentration and the recirculation flow rate, which increases the distribution of liquid along the bed and the accessibility of nitrate to the biomass. The model simulates, as monitored in the industrial anoxic BTF, the increase in the outlet H_2S concentration when the nitrate is depleted in the liquid. Once the availability of the final electron acceptor decreases below the threshold limit, the RE drops instantly until a new cycle starts again with further dosing of nitrate solution (Fig. 3). Soreanu *et al.*[10] detected similar RE drops for nitrate concentrations below 20 g m^{-3} when the inlet load was 4.9 gS $Nm^{-3}\ h^{-1}$ and the TLV was 1.7 m h^{-1}. Depending on the final use of the treated biogas, the fluctuations in H_2S at the outlet could be a significant limitation for its exploitation.

To overcome this drawback, several control strategies have been developed to optimize the BTF performance and these are focused on obtaining the maximum sulfide removal and on optimizing the nitrate dosing with the minimum loss of nitrate in the purge.

Control strategies

The results obtained in the simulation of each control strategy are shown in Table 4. The outlet H_2S concentration and the concentrations of nitrate and sulfide in the recirculation liquid, for the first four CSs, are shown in Fig. 5.

In CS#A, when the nitrate concentration is below 60 gN – NO_3^- m^{-3} the outlet H_2S concentration starts to increase and similar behavior was also observed for sulfide in the recirculation liquid. The nitrate concentration in the discharge liquid for CS#A was 0.07 gN – NO_3^- m^{-3}. CS#A showed the highest maximum outlet H_2S concentration (1.46 gS Nm^{-3}) of the first four control strategies and the lowest amount of nitrate purged during the simulation period.

CS#B showed similar behavior but, as the outlet H_2S concentration was used as a control variable, the maximum outlet H_2S concentration was controlled so that it did not rise above the limit of 0.4 gS Nm^{-3}. Nevertheless, the nitrate concentration in the purged liquid was higher than in CS#A (25.52 gN – NO_3^- m^{-3}) and this represents an undesirable waste of reagent.

In CS#C and CS#D, the addition of the nitrate solution in continuous mode avoids sudden peaks in the outlet H_2S concentration (Fig. 5). In CS#C, the nitrate concentration was in the range 11.9 – 80.8 gN – NO_3^- m^{-3} depending on the inlet sulfide concentration. The outlet H_2S concentration was constant and was equal to 0.4 gS $m^3\ h^{-1}$. The sulfide in the liquid recirculation medium showed similar behavior to that observed with the nitrate. In CS#D, the use of sulfide concentration in the liquid as a variable to control the flow of the nitrate solution allowed a constant sulfide concentration to be achieved in the liquid phase (Fig. 5(C)). As shown in

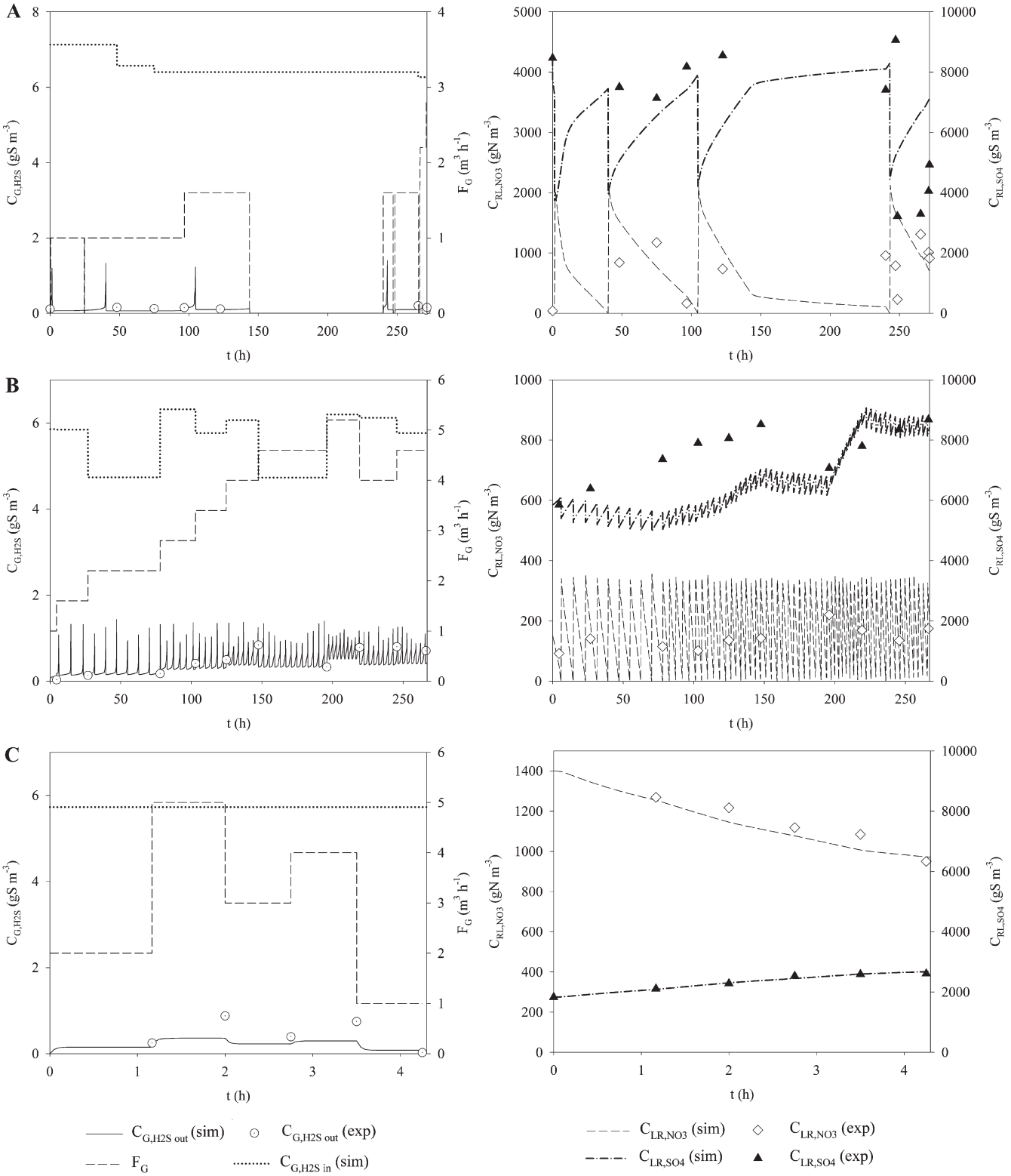

Figure 3. Validation: (A) first experiment; (B) second experiment; (C) third experiment.

Fig. 5(A) for CS#D, when the inlet H_2S concentration was low, the base outlet H_2S concentration was the highest. This unexpected behavior is related to the lower nitrate concentration in the liquid phase (Fig. 5(B)), which is fixed by the constant sulfide concentration in the liquid medium (Fig. 5(C)).

In CS#E and CS#F (Fig. 6(A)), the biogas flow rate was increased if the outlet H_2S concentration did not rise above the limit of 0.36 gS Nm^{-3}. The fluctuations in the biogas flow rate could have two consequences. First, the BTF could work at maximum load regardless of the inlet H_2S concentration. Second, the biogas flow

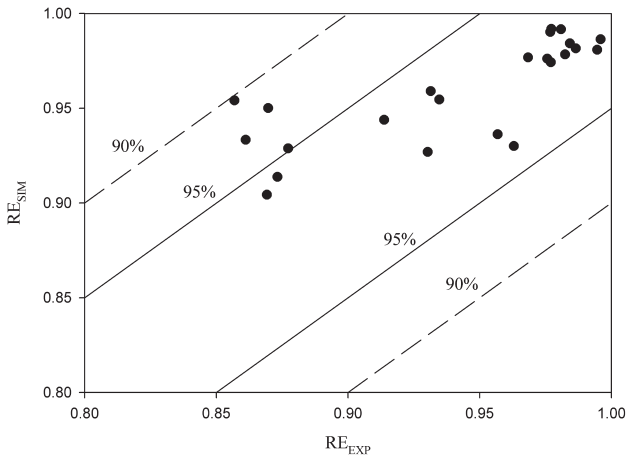

Figure 4. Experimental RE against simulated RE for the three validation experiments.

rate could decrease when the nitrate concentration is low in order to minimize the nitrate purged. In these cases (CS#E and CS#F), the nitrate concentration in the purge liquid was lower than in CS#A and CS#B. More specifically, the nitrate concentration in the purge liquid was 2.9×10^{-4} and 1.65 $gN-NO_3^-\ m^{-3}$ for CS#E and CS#F, respectively. The duration of the peaks in the outlet H_2S concentration, produced as a result of the discontinuous mode, was reduced in this case but the maximum outlet H_2S concentration was not reduced (1.47 and 0.38 gS Nm^{-3} for CS#E and CS#F, respectively). The sulfide concentrations for CS#E and CS#F are shown in Fig. 6(B). In both cases, the sulfide concentration was stable and equal to 4.7 gS m^{-3}, except when nitrate dosing occurred. Just before nitrate dosing, the sulfide concentration decreased to 3 gS m^{-3} due to the decrease in the biogas flow rate. When the nitrate dosing was controlled by the sulfide concentration (CS#E) the sulfide concentration increased to 10 gS m^{-3}. However, for CS#F an increase in the sulfide concentration, caused by the nitrate depletion, was not observed.

Very few studies have been carried out on CS for biogas desulfurization in anoxic BTFs and those that have include a programmed feeding routine[8] and an automatic nitrate dosing using ORP[9]. In this sense, Fernández *et al.*[8] found that the critical elimination capacity (EC) was 30% higher on using a programmed nitrate feed than for manual nitrate dosing. In the programmed feeding routine, the flow of nitrate solution was varied manually according to the H_2S inlet load. Monitoring of the automatic nitrate dosing by ORP has been carried out by Fernández *et al.*[9] This operation mode is closely represented by the case CS#A. Measurement of the electron acceptor concentration as the control variable has recently been implemented in an aerobic BTF for biogas desulfurization.[7] In contrast, in the work described here the electron acceptor was nitrate and an ion-selective electrode (ISE) could therefore be used to measure the nitrate concentration. However, interference with sulfide is the most significant drawback for the use of this method.[8] In the present work, all of the CSs proposed involve model-based feedback control in order to avoid the limitation of the feed-forward control system, which is more sensitive to unpredictable perturbations.[34]

Among the CSs analyzed, when nitrate is dosed in discontinuous mode and the flow rate is constant, CS#A is the most economical strategy because less sophisticated equipment is required to control the operation and the nitrate purged is the lowest (Table 4). Operating at low nitrate concentrations means a higher fluctuation in the H_2S outlet concentration and this periodically reaches values in excess of 1 gS Nm^{-3}. In contrast, when it is necessary to reduce the outlet H_2S concentration peaks, the control mode used in CS#B should be chosen because the outlet H_2S concentration peaks are buffered. Nevertheless, in CS#B a higher amount nitrate is purged (from 0.3 to 5 gN). The EC achieved in the CS#B case is slightly higher than in the first option (0.2 gS $m^{-3}\ h^{-1}$ higher) and markedly higher than those in the rest of the control modes at constant flow rate (up to 2% higher). However, the amount of nitrate that is not used is almost 17 times higher than in CS#A.

When the main requirement of the facility is to ensure a constant H_2S RE the best option is CS#C. The nitrate purged is higher than in cases CS#A and CS#B, but the outlet H_2S concentration is stable. It can be seen in Fig. 5 that the fluctuations in outlet concentrations are completely smoothed but the EC is consequently lower. Moreover, it is expected that the continuous dosing of nitrate will reduce stress on the microbial population, which is subjected to periodic starvation when discontinuous dosing is applied – as widely reported for aerobic biofilters.[35,36]

If the main purpose of the facility is to treat the maximum load possible without reducing the performance of the BTF, strategies CS#E and CS#F should be considered. In these cases, the biogas flow rate is adjusted when the inlet H_2S concentration decreases in order to maximize the inlet load (Fig. 6(A)) prior to biogas storage. Besides, the predicted EC is higher by up to 30% in comparison with the rest of the strategies (Table 4). This finding is consistent with the increase in the load treated. CS#E and CS#F are interesting alternatives when biogas can be stored before its energy exploitation. The choice of H_2S outlet or sulfide concentration as the control variable gives rise to marked differences in terms of operation (Fig. 6(A)). Furthermore, CS#E and CS#F affect the instrumentation required for the control system and, therefore, the installation cost.

Table 4. Outlet sulfide gas concentration mean and maximum; biogas flow rate; inlet load; elimination capacity; amount of nitrate added, purged and spent for each control strategy

	CS#A	CS#B	CS#C	CS#D	CS#E	CS#F
$C_{H2S,OUT}$ (mean) [gS Nm^{-3}]	0.22	0.22	0.4	0.58	0.36	0.35
$C_{H2S,OUT}$ (max) [gS Nm^{-3}]	1.46	0.38	0.4	0.64	1.47	0.38
$F_{G,mean}$ [$m^3\ h^{-1}$]	3	3	3	3	4.75	4.82
L [gS $m^{-3}\ h^{-1}$]	94.1	94.1	94.1	94.1	149.4	151.6
EC [gS $m^{-3}\ h^{-1}$]	90.0	90.1	86.9	83.7	138.9	141.2
$N_{,fed}$ [$gN-NO_3^-$]	920	920	817	737	1380	1380
$N_{,purged}$ [$gN-NO_3^-$]	0.006	2.13	4.55	0.03	4.1×10^{-5}	0.23
$N_{,spent}$ [$gN-NO_3^-$]	811.2	814.4	807.4	736.7	1213.3	1235.5

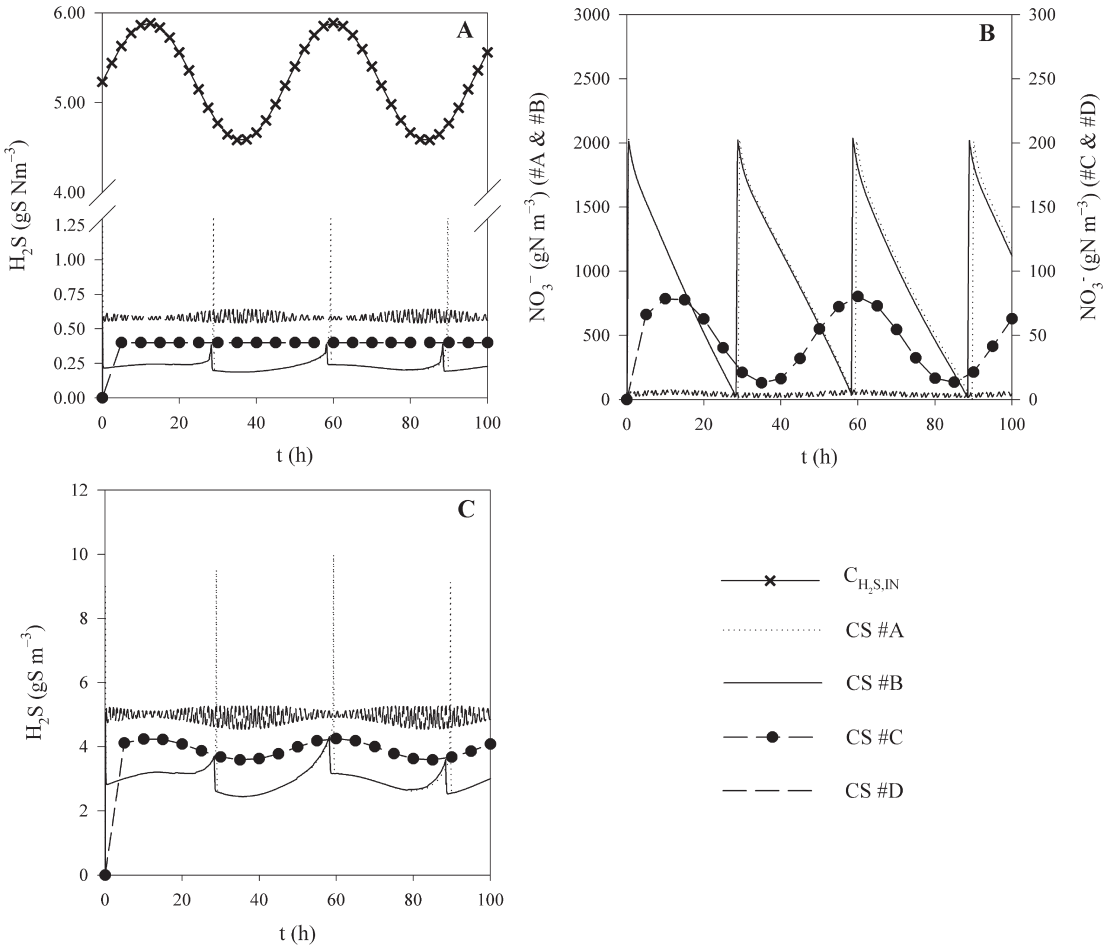

Figure 5. Results of the simulation for CS#A, CS#B, CS#C and CS#D. (A) Outlet H_2S gas concentration; (B) recirculated liquid nitrate concentration; (C) recirculated liquid sulfide concentration.

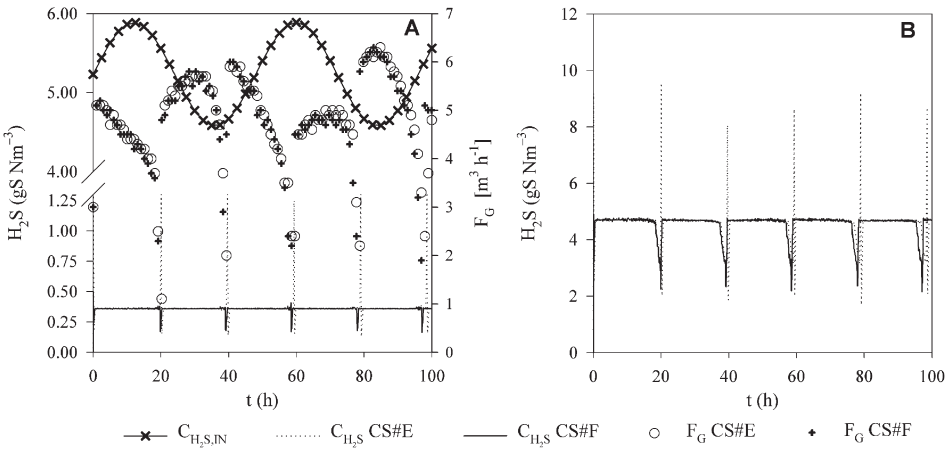

Figure 6. Simulation results for CS#E and CS#F. (A) Outlet H_2S gas concentration and biogas flow rate. (B) Recirculated liquid sulfide concentration.

However, outlet H_2S concentration is controlled in a satisfactory manner and the nitrate purged is the minimum possible.

CONCLUSIONS

The analysis of the different control strategies suggested in the work presented here shows that the best option depends on the characteristics of each individual scenario. However, the mathematical model developed from the description of the phenomena involved in the process is a powerful tool to evaluate all possible strategies when considering and quantifying the savings and improvements in different operation modes. Furthermore, as the model has been calibrated and validated with data obtained by monitoring an industrial plant located in a WWTP, one can expect a high level of fitting between the behavior predicted and the results reported. The mathematical model

described here can be easily adapted to the specific characteristics of each plant and can be used to analyze more efficient control strategies.

ACKNOWLEDGEMENTS

The authors wish to express their sincere gratitude to the Spanish Ministry of Science and Innovation and the European FEDER funds for providing financial support through projects CTM2012-37927-C03 and CTM2012-37927-C02, the Research Result Transfer Office of the University of Cádiz for support of this work through the project 'Procedure for inoculation of industrial biotrickling filters' (PROTO-05-2010) and WWTP 'UTE EDAR Bahía de Cádiz'.

Supporting Information

Supporting information may be found in the online version of this article.

REFERENCES

1 Rasi S, Läntelä J and Rintala J, Trace compounds affecting biogas energy utilisation - a review. *Energ Convers Manage* **52**:3369–3375 (2011)
2 Woodcock KE and Gottlieb M, Gas, natural, in *Kirk-Othmer Encyclopedia of Chemical Technology*. John Wiley & Sons, New York (2000).
3 Abatzoglou N and Boivin S, A review of biogas purification processes. *Biofuel Bioprod Biores* **3**:42–71 (2009).
4 Fortuny M, Gamisans X, Deshusses MA, Lafuente J, Casas C and Gabriel D, Operational aspects of the desulfurization process of energy gases mimics in biotrickling filters. *Water Res* **45**:5665–5674 (2011).
5 Montebello AM, Baeza M, Lafuente J and Gabriel D. Monitoring and performance of a desulphurizing biotrickling filter with an integrated continuous gas/liquid flow analyser. *Chem Eng J* **165**:500–507 (2010).
6 Montebello AM, Fernández M, Almenglo F, Ramírez M, Cantero D, Baeza M and Gabriel D, Simultaneous methylmercaptan and hydrogen sulfide removal in the desulfurization of biogas in aerobic and anoxic biotrickling filters. *Chem Eng J* **200–202**:237–246 (2012).
7 Rodriguez G, Dorado AD, Fortuny M, Gabriel D and Gamisans X, Biotrickling filters for biogas sweetening: oxygen transfer improvement for a reliable operation. *Process Safe Environ* **92**:261–268 (2014).
8 Fernández M, Ramírez M, Gómez JM and Cantero D, Biogas biodesulfurization in an anoxic biotrickling filter packed with open-pore polyurethane foam. *J Hazard Mater* **264**:529–535 (2014).
9 Fernández M, Ramírez M, Pérez RM, Gómez JM and Cantero D, Hydrogen sulphide removal from biogas by an anoxic biotrickling filter packed with Pall rings. *Chem Eng J* **225**:456–463 (2013).
10 Soreanu G, Béland M, Falletta P, Edmonson K and Seto P, Investigation on the use of nitrified wastewater for the steady-state operation of a biotrickling filter for the removal of hydrogen sulphide in biogas. *J Environ Eng Sci* **7**:543–552 (2008).
11 Syed M, Soreanu G, Falletta P and Béland M, Removal of hydrogen sulfide from gas streams using biological processes - a review. *Can Biosyst Eng* **48**:2.1–2.14 (2006).
12 Almenglo F, Ramírez M, Gómez JM and Cantero D, H2S removal from biogas by a pilot anoxic biotrickling filter. Effect of flow rate of biogas and recirculation medium, in *5th IWA Conference on Odors and Air Emissions jointly held with 10th Conference on Biofiltration for Air Pollution Control*. International Water Association, San Francisco, California, USA, paper#43 (2013).
13 Soreanu G, Falletta P, Béland M, Edmonson K, Ventresca B and Seto P, Empirical modelling and dual-performance optimisation of a hydrogen sulphide removal process for biogas treatment. *Bioresource Technol* **101**:9387–9390 (2010).
14 Zarook SM, Shaikh AA and Ansar Z, Development, experimental validation and dynamic analysis of a general transient biofilter model. *Chem Eng Sci* **52**:759–773 (1997).
15 Okkerse WJH, Ottengraf SPP, Osinga-Kuipers B and Okkerse M, Biomass accumulation and clogging in biotrickling filters for waste gas treatment. Evaluation of a dynamic model using dichloromethane as a model pollutant. *Biotechnol Bioeng* **63**:418–430 (1999).
16 Martin RW, Mihelcic JR and Crittenden JC, Design and performance characterization strategy using modeling for biofiltration control of odorous hydrogen sulfide. *J Air Water Manage Assoc* **54**:834–844 (2004).
17 Almenglo F, Ramírez M, Gómez JM and Cantero D, Anoxic biotrickling filter for hydrogen sulfide removal at pilot scale: operational conditions for start-up, in: *BIOMENVI I Workshop on Bioprocess for the Mining Industry and Environmental*, ed by Bevilaqua D, Benedetti AV and Cantero D. UNESP, Araraquara, Sao Paulo, 41–54 (2011).
18 Clesceri LS, Greenberg AE and Eaton AD, *Standard methods for the examination of water and wastewater*. American Public Health Association, Washington DC, 1325 (1999).
19 Almenglo F, Ramírez M, Gómez JM and Cantero D, H2S removal from biogas by a pilot anoxic biotrickling filter. A comparison between co-current and counter-current flow operation mode increasing the loading rate, in *5*th IWA Conference on Odors and *Air Emissions jointly held with 10th Conference on Biofiltration for Air Pollution Control*. International Water Association, San Francisco, California, USA, paper#44 (2013).
20 An S, Tang K and Nemati M, Simultaneous biodesulphurization and denitrification using an oil reservoir microbial culture: effects of sulphide loading rate and sulphide to nitrate loading ratio. *Water Res* **44**:1531–1541 (2010).
21 Mora M, Fernández M, Gómez J, Cantero D, Lafuente J, Gamisans X and Gabriel D, Kinetic and stoichiometric characterization of anoxic sulfide oxidation by SO-NR mixed cultures from anoxic biotrickling filters. *Appl Microbiol Biotechnol* **99**:77–87 (2015).
22 Alonso C, Suidan MT, Kim BR and Kim BJ, Dynamic mathematical model for the biodegradation of VOCs in a biofilter: biomass accumulation study. *Environ Sci Technol* **32**:3118–3123 (1998).
23 Baltzis BC, Mpanias CJ and Bhattacharya S, Modeling the removal of VOC mixtures in biotrickling filters. *Biotechnol Bioeng* **72**:389–401 (2001).
24 Kim S and Deshusses MA, Development and experimental validation of a conceptual model for biotrickling filtration of H2S. *Environ Prog* **22**:119–128 (2003).
25 Zhu XQ, Alonso C, Suidan MT, Cao HW, Kim BJ and Kim BR, The effect of liquid phase on VOC removal in trickle-bed biofilters. *Water Sci Technol* **38**:315–322 (1998).
26 Onda K, Takeuchi H and Okumoto Y, Mass transfer coefficients between gas and liquid phases in packed columns. *J Chem Eng Jpn* **1**:56–62 (1968).
27 Fuller EN, Schettler PD and Giddings JC, A new method for prediction of binary gas-phase diffusion coefficients. *Ind Eng Chem* **58**:18–27 (1966).
28 Wilke CR, Diffusional properties of multicomponent gases. *Chem Eng Prog* **46**:95–104 (1950).
29 Boudreau BP, *Diagenetic Models and their Implementation: Modelling Transport and Reactions in Aquatic Sediments*. Springer, Berlin, New York (1997).
30 Li YH and Gregory S, Diffusion of ions in sea-water and in deep-sea sediments. *Geochim Cosmochim Acct* **38**:703–714 (1974).
31 De Bruyn WJ, Swartz E, Hu JH, Shorter JA, Davidovits P, Worsnop DR, Zahniser MS and Kolb CE, Henry's law solubilities and Śetchenow coefficients for biogenic reduced sulfur species obtained from gas–liquid uptake measurements. *J Geophys Res - Atmos* **100**:7245–7251 (1995).
32 Perrin DD, *Pure IUo and Data ACCoE, Ionisation Constants of Inorganic Acids and Bases in Aqueous Solution*. Pergamon Press (1982).
33 API, *Technical Data Book-Petroleum Refining*, 6th edn. American Petroleum Institute (1997).
34 Cervin A, Eker J, Bernhardsson B and Årzén K-E, Feedback–feedforward scheduling of control tasks. *Real-Time Syst* **23**:25–53 (2002).
35 Moe W and Li C, A design methodology for activated carbon load equalization systems applied to biofilters treating intermittent toluene loading. *Chem Eng J* **113**:175–185 (2005).
36 Dorado AD, Lafuente J, Gabriel D and Gamisans X, Interaction between sorption and biodegradation in a biofilter packed with activated carbon. *Water Sci Technol* **66**:1743–1750 (2012).

